ACS APPLIED MATERIALS & INTERFACES

Research Article

www.acsami.org

Chemical Adsorption Enhanced CO_2 Capture and Photoreduction over a Copper Porphyrin Based Metal Organic Framework

Yuanyuan Liu,[†] Yanmei Yang,[†] Qilong Sun,[‡] Zeyan Wang,[†] Baibiao Huang,*[,†] Ying Dai,[‡] Xiaoyan Qin,[†] and Xiaoyang Zhang[†]

[†]State Key Lab of Crystal Materials, Shandong University, Jinan 250100, People's Republic of China

[‡]School of Physics, Shandong University, Jinan 250100, People's Republic of China

Supporting Information

ABSTRACT: Effective CO_2 capture and activation is a prerequisite step for highly efficient CO_2 reduction. In this study, we reported a case of Cu^{2+} in a porphyrin based MOF promoted enhanced photocatalytic CO_2 conversion to methanol. Compared with the sample without Cu^{2+}, the methanol evolution rate was improved as high as 7 times. In situ FT-IR results suggested that CO_2 chemical adsorption and activation over Cu^{2+} played an important role in improving the conversion efficiency.

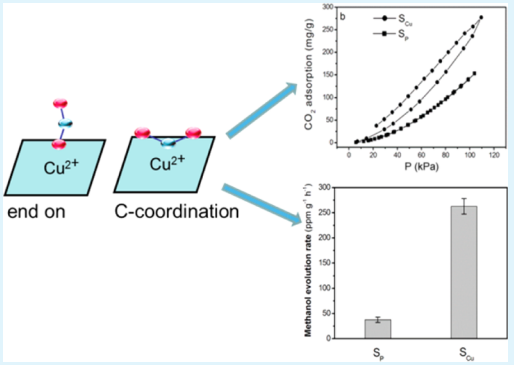

KEYWORDS: *photocatalysis, CO_2 capture, CO_2 reduction, chemical adsorption, and MOFs*

1. INTRODUCTION

The energy crisis and global warming are two severe problems worldwide. CO_2 has received much attention as one of the primary greenhouse gases. Its conversion to valuable fuels offers a way to alleviate the above two problems. Photocatalytic conversion of CO_2 by utilizing solar energy is regarded as one of the most green and economic methods. Up to now, conversion of CO_2 into small organic molecules (i.e., carbon oxide, methane, methanol, ethanol, etc) over various photocatalysts has been reported, such as TiO_2,[1] $BiVO_4$,[2] Bi_2WO_6,[3] Zn_2GeO_4,[4] etc. However, the efficiency is still low, since CO_2 is a highly stable molecule. The C═O bond energy in CO_2 is 750 kJ/mol, much higher than that of C−C (336 kJ/mol), C−O (327 kJ/mol), and C−H (411 kJ/mol). Therefore, effective CO_2 capture and activation is a prerequisite step for highly efficient CO_2 reduction. Oxygen vacancy was reported to enable $SrTiO_3$ to chemically adsorb and activate CO_2, which would lower the energy barrier of CO_2 and facilitate the subsequent photoreduction.[5]

Coordination to transition metals is another known method to activate CO_2, which results in a net transfer of electron density from the metal to the LUMO of CO_2. The LUMO of CO_2 is an antibonding orbital, and therefore, electron transfer should result in a weakened C−O interaction.[6] Copper organic complexes are well-known for their assistance in CO_2 capture and activation.[7,8] For example, Angamuthu reported a copper complex, which could spontaneously capture and reductively couple CO_2 from air, yielding an oxalate-bridged copper tetramer in acetonitrile solution.[9] Liu reported that copper ions in TiO_2 could help the activation of CO_2 via the coordination with the π orbital of CO_2 and enhance the adsorbed CO_2^- dissociation.[10] In addition, copper-containing photocatalysts were reported to be able to improve the CO_2 capture capability and photocatalytic activity, because Cu appeared to be active toward CO_2 adsorption and photoreduction. Yang et al. reported that both the CO_2 capture capability and the photocatalytic activity of ZIF-67 were improved by doping Cu to ZIF-67.[11] Cu-containing LDHs were also found to display better performance than those without Cu.[12,13]

Porphyrins are important naturally occurring organic compounds, and widely applied in dye-sensitized solar cells and photodynamic therapy, etc.[14−16] Co porphyrin and Fe porphyrin have been well-studied for their photocatalytic and electrocatalytic activity in CO_2 reduction as homogeneous catalysts.[17,18] Recently, Fateeva synthesized a water stable metal organic framework (MOFs) using porphyrin and Al^{3+}, and the as-prepared sample was found to display photocatalytic activity toward hydrogen production from water.[19] MOFs are a class of crystalline micromesoporous hybrid materials with an extended 3D network and have drawn extensive research interests in recent years due to their large surface areas, tunable porous structures, desired functionality, and promising capacity for CO_2 capture.[20,21] In addition, MOFs are heterogeneous photocatalysts, which can be easily recycled.

Received: May 23, 2013
Accepted: June 28, 2013
Published: June 28, 2013

In this study, we mimic the photosynthesis using a Cu porphyrin (5,10,15,20-tetrakis(4-carboxyphenyl) porphyrin, TCPP) based MOF (denoted as S_{Cu}). S_{Cu} exhibits better performances of both CO_2 capture and photocatalytic CO_2 conversion to methanol than the samples without Cu (denoted as S_P). The presence of Cu induces chemical adsorption of CO_2 on S_{Cu}, as identified by FT-IR characterization. Through chemical adsorption, CO_2 activation is achieved, which results in enhanced CO_2 capture capability and higher photoreduction efficiency.

2. EXPERIMENTAL SECTION

2.1. Materials. All reagents were analytical grade and were used without further purification. 5,10,15,20-Tetrakis(4-carboxyphenyl) porphyrin (TCPP) was purchased from TIC.

2.2. Synthesis of S_P and S_{Cu}. S_P and S_{Cu} were synthesized according to the literature.[19]

Synthesis of S_P. A 200 mg portion of (TCPP) and 120 mg of $AlCl_3 \cdot 6H_2O$ were introduced into 20 mL of deionized water. The suspension was stirred for 30 min at room temperature and then transferred into a 80 mL Teflon-lined autoclave and kept at 180 °C for 24 h. After cooling down to room temperature, the solid was centrifuged, and washed with DMF and acetone several times. Finally, the obtained power was dried at 60 °C.

Synthesis of S_{Cu}. A 2 mmol portion of $CuSO_4 \cdot 5H_2O$ was dissolved into 20 mL of DMF, and 50 mg of S_P was added into the solution. The mixture was allowed to react at 100 °C for 48 h. The resulting solid was washed with DMF and water several times, and dried at 60 °C.

2.3. Characterizations. X-ray power diffraction analysis (XRD) of the samples was recorded on an X-ray diffractometer (Bruker AXS D8). The morphology and microstructure and energy dispersive spectra (EDS) of the sample were determined by scanning electron microscopy (SEM, Hitachi S-4800 microscope), and its diffuse reflectance spectra (DRS) by UV/visible spectroscopy (UV-2550, Shimadzu). The chemical states of the samples were characterized by XPS (Thermo Fisher Scientific Escalab 250), and C 1s (284.6 eV) was used to calibrate the peak positions. A Micromeritics ASAP 2020 apparatus was used to measure the BET surface area and the pore-size distributions. CO_2 adsorption/desorption measurements were conducted under the ambient condition of 298 K at low pressure (1 atm, Builder SSA-4200C), and the pressure can be altered stepwise by the gas flow rate. In situ Fourier transform infrared (FT-IR) spectra were recorded using an in situ sample cell, an accessory of the FT-IR spectrometer (Nicolet Nexus 670). The window in the in situ sample cell is ZnSe. The spectra were detected at room temperature (25 °C) and 1 atm. Before spectra detection, the samples were under heat treatment at 100 °C under vacuum overnight to remove the adsorbed gas molecules from the air, and CO_2 was slowly inlet into the sample cell for an hour before the cell was sealed.

2.4. Photocatalytic CO_2 Reduction Evaluation. In the photocatalytic conversion of CO_2, 30 mg of S_P or S_{Cu} was dispersed in 100 mL of water containing 1 mL of triethylamine (TEA) with magnetic stirring, and high-purity CO_2 gas was continuously bubbled through the solution at the rate of 0.2 mL min^{-1}. A 300 W Xe arc lamp (PLS-SXE300, Beijing Trusttech Co., Ltd.) equipped with an ultraviolet cutoff filter to provide visible light ($\lambda \geq 420$ nm) was used as the light source. The photocatalytic CO_2 reduction experiments were conducted in a closed vessel at 5 °C, and the suspensions were irradiated through the quartz window. Prior to irradiation, CO_2 gas was bubbled to the solution for 10 min to expel the dissolved air in the vessel. The solution products were qualitatively analyzed by a Varian CP-3800 gas chromatograph (FID detector, Propark Q column) through observing and comparing the chromatographic peaks with those for the authentic methanol standard. The injection temperature was 100 °C, and the detection temperature was 200 °C. The temperature of the column first remained at 40 °C for 3 min and then increased to 200 °C with a rate of 20 °C/min.

3. RESULTS AND DISCUSSION

XRD analysis was first carried out to investigate the crystal structure of the as-prepared samples, as can be seen from Figure 1a. All the diffraction peaks for S_P are indexed to an

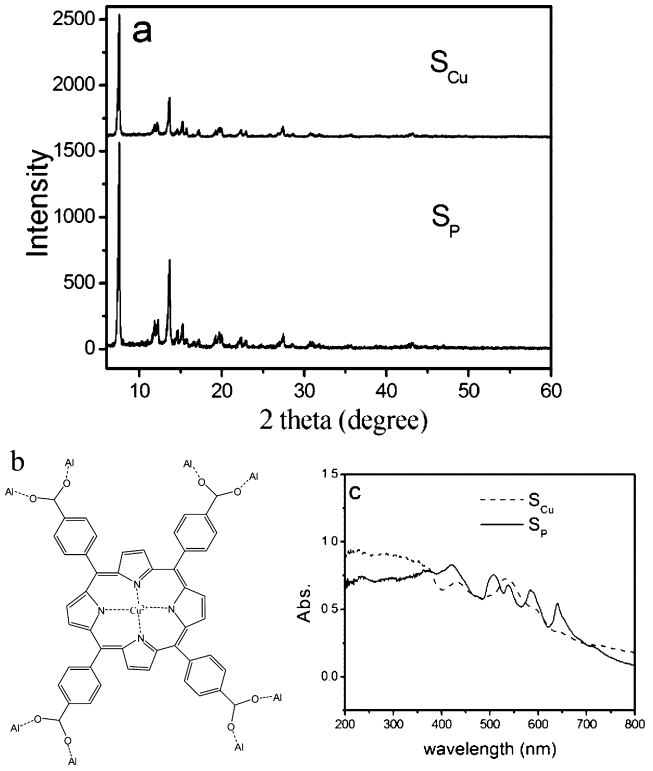

Figure 1. (a) XRD patterns of the as-prepared S_P and S_{Cu}. (b) Linkage of Cu porphyrin to Al^{3+} in S_{Cu}. (c) DRS spectra of S_P and S_{Cu}.

orthorhombic structure with *Cmmm* symmetry, and no impurity peaks are observed.[19] The relatively strong diffraction intensity indicates good crystallinity of S_P. The cell parameters have been known with a = 31.978 Å, b = 6.5812 Å, and c = 16.862. Therefore, the main peaks observed at 2θ = 7.43° and 13.67° could be indexed as the (201) and (110) reflections, respectively. In S_P, each oxygen in the carboxylate group is coordinated with one Al^{3+}, and Al^{3+} coordination consists of four carboxylate-derived oxygen atoms in the equatorial plane and two $\mu 2$ axial OH^- bridging adjacent Al^{3+} centers to form an infinite $Al(OH)O_4$ chain, as shown by Figure 1b. Compared with S_P, the diffraction peaks of S_{Cu} do not change, which suggests that Cu insertion does not destroy the framework structure. However, the intensity of the diffraction peaks decrease, indicating that Cu insertion into the porphyrin has a negative effect on the crystallinity. Additionally, no traces of characteristic peaks corresponding to CuO or Cu_2O are observed in S_{Cu}, indicating that no impurity is introduced after Cu insertion.

Figure 1c shows the DRS spectra of S_P and S_{Cu}. As can be seen, both S_P and S_{Cu} display strong absorption from 200 to 800 nm. S_P displays a strong S band and four Q bands, which are characteristic for the porphyrin family. After the metalation of the porphyrin ring with Cu^{2+}, the four Q bands in S_{Cu} become two due to the higher symmetry of S_{Cu}. Compared with S_P, S_{Cu} displays a slight red shift of the S band (from 420 to 430 nm), which is a common phenomenon for metalated porphyrin.[22] Analysis of the SEM image shows that both S_{Cu}

dx.doi.org/10.1021/am4019675 | ACS Appl. Mater. Interfaces 2013, 5, 7654−7658

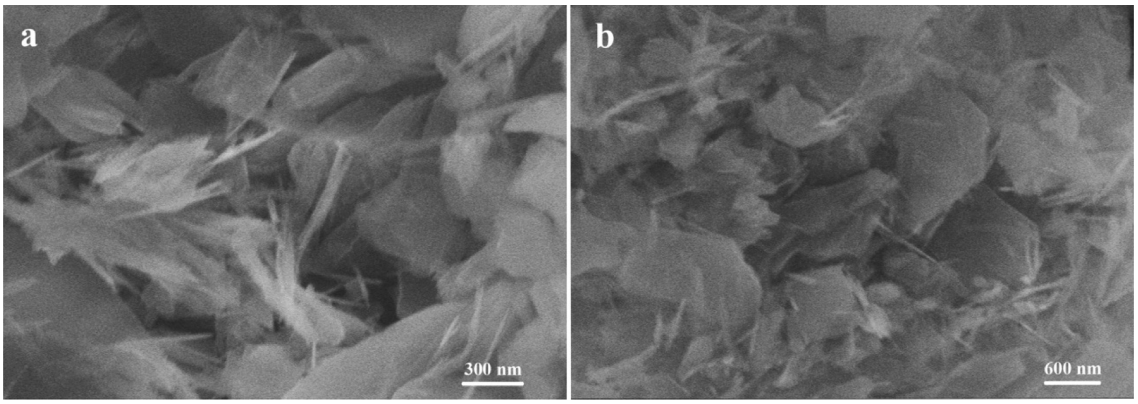

Figure 2. SEM images of S_{Cu} (a) and S_P (b).

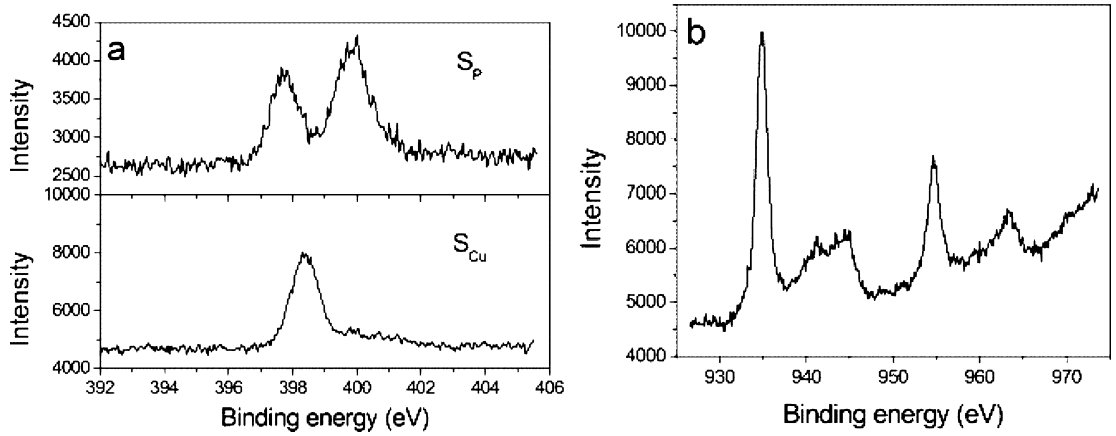

Figure 3. XPS spectra of the as-prepared samples: (a) N 1s spectra of S_P and S_{Cu}, and (b) Cu 2p spectra of S_{Cu}.

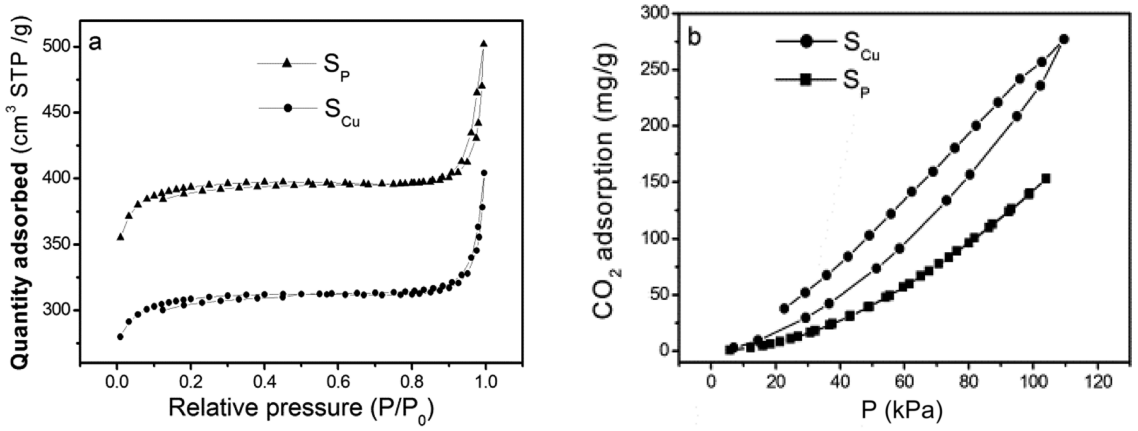

Figure 4. (a) N_2 adsorption−desorption isotherms and (b) CO_2 adsorption and desorption isotherms of S_{Cu} and S_P.

and Sp are composed of nanoplates, with a thickness of 20−30 nm. No distinguishable difference can be observed between S_P and S_{Cu} (Figure 2). The energy-dispersive spectrum (EDS) displays an Al/Cu ratio of 2, indicating 100% occupancy of the porphyrin center sites by Cu^{2+} (Figure S1, Supporting Information).

XPS is known to identify the surface composition and local chemical environments of a compound. As can be seen from the structure, the free base porphyrin in S_P contains two chemically different types of nitrogen atoms, (=N−, and −NH). After the introduction of Cu into the porphyrin ring, however, all the nitrogen atoms in porphyrin bind to Cu ions. Thus, there should be one N 1s signal. The N 1s XPS spectra of as-prepared S_P and S_{Cu} are displayed in Figure 3a. Obviously, two signals for S_P at 399.9 and 397.7 eV are observed, which are ascribed to −NH− and =N−, respectively. For S_{Cu}, only one signal at 398.4 eV is detected, which is in good agreement with the above discussion. Therefore, it can be concluded that Cu indeed inserted into the porphyrin ring. Figure 3b shows the Cu 2p spectra of S_{Cu}. The Cu 2p 3/2 and 1/2 locate at 934.9 and 954.8 eV, respectively, each peak with a broad satellite structure toward higher binding energies. It was reported that the satellite peak was due to the open-shell 3d character of

dx.doi.org/10.1021/am4019675 | ACS Appl. Mater. Interfaces 2013, 5, 7654−7658

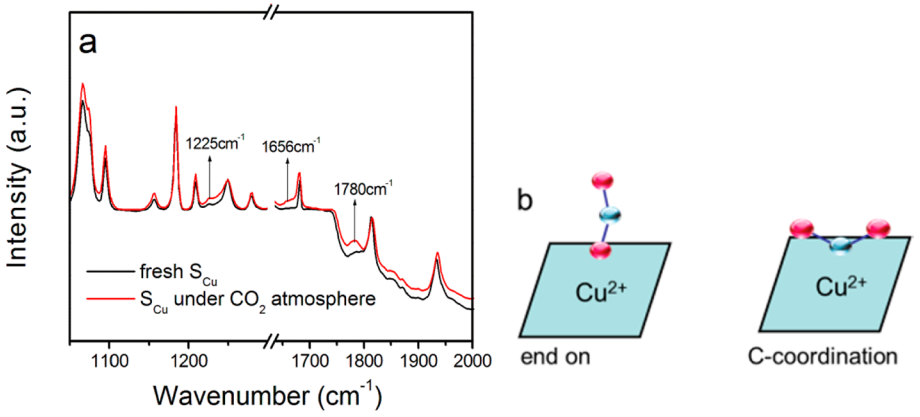

Figure 5. (a) In situ FT-IR spectra of fresh S_{Cu} and S_{Cu} under a CO_2 atmosphere. (b) Schematic representation of "end-on" and "C-coordination" adsorption geometry of CO_2 on S_{Cu}.

Cu^{2+}. Both the binding energy and the peak shape of Cu 2p suggest that Cu remains in its 2^+ valence state in S_{Cu}.[23,24]

Figure 4a shows the nitrogen adsorption−desorption isotherms measured at liquid nitrogen temperature. Both S_P and S_{Cu} exhibit a typical type II N_2 adsorption isotherm, which is often observed in nonporous materials or materials with macropores or open voids.[25] This is in good agreement with the framework structure of S_{Cu} and S_P, which display two distinct channels (6 × 11 Å elliptical pore and 5 Å rectangular pore). The Brunauer−Emmett−Teller (BET) surface areas were 1187 and 932 cm^2/g for S_P and S_{Cu}, respectively. The smaller BET surface area of S_{Cu} could be due to the insertion of Cu^{2+} into porphyrin, which blocks the porphyrin pores in S_P. The pore volume is 0.625 and 0.776 cm^3/g for S_{Cu} and S_P, respectively. The smaller pore volume of S_{Cu} again indicates the Cu insertion into the porphyrin ring. According to the CO_2 adsorption−desorption isotherm shown in Figure 4b, the amount of CO_2 adsorption capacity over S_{Cu} is 277.4 mg/g (1 atm, 298 K), which is much higher than that of Sp (153.1 mg/g). This result is consistent with that reported in the literature; that is, at $P < 1$ bar, CO_2 uptake is not related to surface area.[26] Rosi synthesized metal-adeninate based MOFs, showing a CO_2 uptake capacity of 4.5 mmol/g at 1 atm (ca. 198 mg/g).[27] Snurr systematically investigated 14 M/DOBDC MOFs, and the biggest CO_2 uptake was about 350 mg/g.[28] Obviously, our results are comparable with the reported results. The desorption process is completely reversible over S_P, indicating physical interaction between CO_2 and S_P. In contrast, the desorption process over S_{Cu} is irreversible, which stops at 20 kPa and results in an unclosed loop. The adsorption−desorption cycle is repeated three times, and no noticeable changes are observed for S_P. However, the unclosed loop is observed at each run for S_{Cu}, suggesting that it is not an accidental phenomenon (Figure S2, Supporting Information). As we all know, the hysteresis loop is normally induced by the capillary action. However, the possibility that capillary action induced the unclosed loop for S_{Cu} can be ruled out considering the two facts: (1) S_{Cu} has the same framework structure as S_P, and (2) the unclosed loop is not observed for S_P. The open adsorption−desorption isotherm of S_{Cu} could indicate the chemical adsorption of CO_2 on S_{Cu}, which is also accordant with the enhanced adsorption capacity for S_{Cu}.

The chemical adsorption of CO_2 on S_{Cu} was confirmed by FT-IR measurements, which is widely used to monitor the interaction between a gas and a solid. As can be seen in Figure 5a, S_{Cu} under a CO_2 atmosphere displays three new peaks at 1780, 1656, and 1225 cm^{-1}, compared with fresh S_{Cu}. The peaks at 1780 and 1656 cm^{-1} are due to the asymmetric stretching vibrations ν_{as}(OCO) of the "end-on" and "C-coordination" coordination states, respectively (Figure 5b). The peak at 1225 cm^{-1} corresponds to the symmetric stretching vibration of CO_2 for both of the two coordination modes on S_{Cu}.[29] No changes are observed from the FT-IR spectra for fresh S_P and S_P under a CO_2 atmosphere (Figure S3, Supporting Information). This indicated that CO_2 could be chemically adsorbed on S_{Cu} at the Cu site by the "end on" or "C-coordination" mode. It is noteworthy that, due to the chemical adsorption, the linear CO_2 molecules would bend, which is believed to lower the reaction barrier and, therefore, improve the photocatalytic efficiency during the photoreduction process.

To verify the above assumption, photocatalytic CO_2 reduction was carried out in aqueous solutions under visible light irradiation. Methanol is the predominant product during the photocatalytic reaction. As expected, the methanol evolution rate for S_P is 37.5 ppm g^{-1} h^{-1}, while that for S_{Cu} is 262.6 ppm g^{-1} h^{-1}, about as high as 7 times that of S_P (Figure S4, Supporting Information). This result confirms the above discussion; that is, CO_2 chemical adsorption on Cu^{2+} in S_{Cu} is beneficial for high photoreduction efficiency.

To exclude the influences of other factors during the photocatalytic experiments, three control experiments were also carried out: (1) N_2 instead of CO_2 was introduced; (2) with visible light irradiation, but without photocatalysts; (3) with photocatalyst, but without visible light irradiation. Negligible methanol is detected in the above three experiments, indicating that methanol generation is really based on the photopromoted reduction of CO_2.

4. CONCLUSION

In conclusion, the assumption of CO_2 activation and its benefit for subsequent photoreduction is proved via a Cu porphyrin based MOF. The presence of Cu in a porphyrin based MOF promotes CO_2 chemical adsorption and activation, as evidenced by CO_2 adsorption curves and FT-IR spectra. The CO_2 chemical adsorption bends the linear CO_2 molecule, and is believed to lower the photoreduction barrier and, consequently, improve the efficiency. This study highlights the importance of CO_2 chemical adsorption on a photocatalyst in improving the photocatalytic activity, which provides a strategy for designing

dx.doi.org/10.1021/am4019675 | ACS Appl. Mater. Interfaces 2013, 5, 7654−7658

efficient photocatalysts for CO_2 capture and reduction in the future.

■ ASSOCIATED CONTENT

Supporting Information

EDS spectra, CO_2 adsorption−desorption cycles, in situ FT-IR spectra, and methanol evolution rate. This material is available free of charge via the Internet at http://pubs.acs.org.

■ AUTHOR INFORMATION

Corresponding Author

*E-mail: bbhuang@sdu.edu.cn.

Notes

The authors declare no competing financial interest.

■ ACKNOWLEDGMENTS

This work is financially supported by the National Basic Research Program of China (No. 2013CB632401), the National Science Foundation of China (Nos. 21007031, 51002091, and 51021062), the Natural Science Foundation of Shandong Province (ZR2010BQ005), and the Specialized Research Fund for the Doctoral Program of Higher Education (20100131120029).

■ REFERENCES

(1) Varghese, O. K.; Paulose, M.; LaTempa, T. J.; Grimes, C. A. *Nano Lett.* **2009**, *9*, 731−737.
(2) Liu, Y. Y.; Huang, B. B.; Dai, Y.; Zhang, X.; Qin, X.; Jiang, M.; Whangbo, M. H. *Catal. Commun.* **2009**, *11*, 210−213.
(3) Cheng, H. F.; Huang, B. B.; Liu, Y. Y.; Wang, Z. Y.; Qin, X.; Zhang, X.; Dai, Y. *Chem. Commun.* **2012**, *48*, 9729−9731.
(4) Liu, Q.; Zhou, Y.; Tian, Z.; Chen, X.; Gao, J.; Zou, Z. *J. Mater. Chem.* **2012**, *22*, 2033−2038.
(5) Xie, K.; Umezawa, N.; Zhang, N.; Reunchan, P.; Zhang, Y.; Ye, J. *Energy Environ. Sci.* **2011**, *4*, 4211−4219.
(6) Leitner, W. *Coord. Chem. Rev.* **1996**, *153*, 257−284.
(7) Sakaki, S.; Kitaura, K.; Morokuma, I. K. *Inorg. Chem.* **1982**, *21*, 160−165.
(8) Caballol, R.; Marcos, E. S.; Barthelat, J.-C. *J. Phys. Chem.* **1987**, *91*, 1328−1333.
(9) Angamuthu, R.; Byers, P.; Lutz, M.; Spek, A. L.; Bouwman, E. *Science* **2010**, *327*, 313−315.
(10) Liu, L.; Zhao, C.; Li, Y. *J. Phys. Chem. C* **2012**, *116*, 7904−7912.
(11) Yang, H.; He, X. W.; Wang, F.; Kang, Y.; Zhang, J. *J. Mater. Chem.* **2012**, *22*, 21849−21851.
(12) Ahmed, N.; Shibata, Y.; Taniguchi, T.; Izumi, Y. *J. Catal.* **2011**, *279*, 123−135.
(13) Ahmed, N.; Morikawa, M.; Izumi, Y. *Catal. Today* **2012**, *185*, 263−269.
(14) Ambre, R.; Chen, K. B.; Yao, C. F.; Luo, L.; Diau, E. W.; Hung, C. H. *J. Phys. Chem. C* **2012**, *116*, 11907−11916.
(15) Bonnett, R. *Chem. Soc. Rev.* **1995**, 19−33.
(16) Gao, B.; Liu, Y.; Yin, H.; Li, Y.; Baia, Q.; Zhang, L. *New J. Chem.* **2012**, *36*, 28−31.
(17) Behar, D.; Dhanasekaran, T.; Neta, P.; Hosten, C. M.; Ejeh, D.; Hambright, P.; Fujita, E. *J. Phys. Chem. A* **1998**, *102*, 2870−2877.
(18) Grodkowski, J.; Behar, D.; Neta, P.; Hambright, P. *J. Phys. Chem. A* **1997**, *101*, 248−254.
(19) Fateeva, A.; Chater, P. A.; Ireland, C. P.; Tahir, A. A.; Khimyak, Y. Z.; Wiper, P. V.; Darwent, J. R.; Rosseinsky, M. J. *Angew. Chem., Int. Ed.* **2012**, *51*, 7440−7444.
(20) Fe′ rey, G.; Serre, C.; Devic, T.; Maurin, G.; Jobic, H.; Llewellyn, P.; Weireld, G. D.; Vimont, A.; Daturif, M.; Chang, J.-S. *Chem. Soc. Rev.* **2011**, *40*, 550−562.
(21) Sumida, K.; Rogow, D. L.; Mason, J. A.; McDonald, T. M.; Bloch, E. D.; Herm, Z. R.; Bae, T. H.; Long, J. R. *Chem. Rev.* **2012**, *112*, 724−781.
(22) Dolphin, D., Ed. *The Porphyrins: Physical Chemistry, Part A*; Academic Press Inc.: New York, 1978; Vol. *III*, p 106.
(23) Karweik, D. H.; Winograd, N. *Inorg. Chem.* **1976**, *15*, 2336−2342.
(24) Carniato, S.; Dufour, G.; Luo, Y.; Ågren, H. *Phys. Rev. B* **2002**, *66*, 045105.
(25) Tsai, W. T.; Yang, J. M.; Lai, C. W.; Cheng, Y. H.; Lin, C. C.; Yeh, C. W. *Bioresour. Technol.* **2006**, *97*, 488−493.
(26) Yang, Q.; Zhong, C.; Chen, J. F. *J. Phys. Chem. C* **2008**, *112*, 1562−1569.
(27) An, J.; Rosi, N. L. *J. Am. Chem. Soc.* **2010**, *132*, 5578−5579.
(28) Yazaydin, A. O.; Snurr, R. Q.; Park, T. H.; Koh, K.; Liu, J.; LeVan, M. D.; I. Benin, A.; Jakubczak, P.; Lanuza, M.; Galloway, D. B.; Low, J. J.; Willis, R. R. *J. Am. Chem. Soc.* **2009**, *131*, 18198−18199.
(29) Wang, Y.; Lafosse, A.; Jacobi, K. *J. Phys. Chem. B* **2002**, *106*, 5476−5482.